Materials Sciences and Applications, 2014, 5, 932-942
Published Online November 2014 in SciRes. http://www.scirp.org/journal/msa
http://dx.doi.org/10.4236/msa.2014.513095

Scientific Research

The Influence of Zn^{2+} Ions Substitution on the Microstructure and Transport Properties of Mn-Zn Nanoferrites

Mohamed Ali Ahmed[1], Kasim El-Sayed Rady[2*], Kamel Mohamed El-Shokrofy[2], Ahmed Abo Arais[3], Mohamed Said Shams[3]

[1]Materials Science Laboratory, Physics Department, Faculty of Science, Cairo University, Giza, Egypt
[2]Engineering Basic Sciences Department, Faculty of Engineering, Menoufia University, Shebin El-Kom, Egypt
[3]Department of Physics and Engineering Mathematics, Faculty of Electronic Engineering, Menoufia University, Al Minufya, Egypt
Email: *k_rady_2001@yahoo.com

Received 19 September 2014; revised 23 October 2014; accepted 4 November 2014

Abstract

The effect of Zn^{2+} ions on the microstructure and electrical properties of $Mn_{1-x}Zn_xFe_2O_4$ ($0.0 \le x \le 0.5$ in steps of 0.1) through a solid state reaction has been investigated. The structural properties have been investigated using X-ray diffraction (XRD) technique. The XRD analysis confirms that all samples are in a single-phase cubic spinel structure. The experimental lattice parameter (a_{exp}) was decreased with increasing Zn^{2+} ions substitution due to the smaller ionic radius of zinc content. The crystallite size (t) of samples was estimated by Scherrer's formula and found in the range (90 - 115 nm). Dc electrical resistivity and Seebeck voltage coefficients were measured as a function of temperature using the two probe methods. The temperature variation of resistivity exhibits two breaks, each break referring to a change in the activation energy. The Curie temperature estimated from dc resistivity measurement decreases with increasing Zn^{2+} ions. Seebeck voltage coefficient measurements reveal n-type conduction for all samples.

Keywords

Mn-Zn Ferrite, XRD, Microstructure, IR, DC Resistivity, Seeback Coefficient

1. Introduction

Soft ferromagnetic oxides are of great importance as high-frequency magnetic materials. The general formula

*Corresponding author.

How to cite this paper: Ahmed, M.A., Rady, K.E.-S., El-Shokrofy, K.M., Arais, A.A. and Shams, M.S. (2014) The Influence of Zn^{2+} Ions Substitution on the Microstructure and Transport Properties of Mn-Zn Nanoferrites. *Materials Sciences and Applications*, **5**, 932-942. http://dx.doi.org/10.4236/msa.2014.513095

for these compounds is $MOFe_2O_3$, where M is a divalent metallic ion such as Fe^{2+}, Ni^{2+}, Mg^{2+}, Mn^{2+}, Zn^{2+} or a mixture of these ions [1]-[3]. Manganese zinc ferrites represent an important class of soft ferromagnetic materials which possesses cubic spinel structure described by the formula $(A)[B]_2O_4$, where (A) and [B] refer to tetrahedral and octahedral cation sites, respectively, in a FCC anion (oxygen) sub-lattice. The type of cations and their distribution between the two interstitial sites in these ferrites determine many of the intrinsic magnetic properties of the ferrites [4] [5].

Manganese zinc ferrites represent an important class of soft ferromagnetic materials characterized by high magnetic permeabilities, wide range of temperature and frequency, and high stability which are widely used in anti-electromagnetic interference (EMI) noise filters, broad band electronic circuits transformers, integrated services digital network (ISDN), local area network (LAN), wide area network (WAN), pulse transformer, and background lighting, etc. [6]. Recently, study on frequency characteristic of high-permeability Mn-Zn ferrites has become one of the hotspots in the research field of magnetic material [7]. Ghazanfar *et al*. [8] in their research showed a decrease of the lattice constant and increasing trend of density with increasing zinc content. Mn-ferrite has a high magnetic properties and relative small resistivity, so we perform this study to increase the resistivity of this ferrite with maintaining the magnetic properties as high as possible by substituting Mn^{2+} ions by Zn^{2+} ions to reduce the electric losses. M.M. Hessien *et al*. [9] in his research showed a decrease of the lattice constant with increasing zinc content. Maximum saturation magnetization (M_s) was obtained at $Mn_{0.8}Zn_{0.2}Fe_2O_4$ phase. S.J. Kim *et al*. [10] studied the thermal variation of MgZn nanoferrites for magnetic hyperthermia, used Mössbauer spectra to show Fe^{3+} and Fe^{2+} valence states and explained that the saturation magnetization was increased by Fe^{2+} ion.

Electrical transport properties of ferrites provide information suitable for the selection of these materials for specific application and they are used in the interpretation of the conduction mechanism in semiconductors. The measurement of thermoelectric power is simple and its sign gives vital information about the type of conduction in semiconductors, *i.e*., whether they are n- or p-type. Electrical conductivity, which gives valuable information about conduction mechanism, is one of the important properties of ferrites [11] [12].

In this work, we study the influence of Zn^{2+} ions substitution on the microstructure and transport properties of $Mn_{1-x}Zn_xFe_2O_4$ ($0.0 \le x \le 0.5$ in steps of 0.1) using X-ray diffraction (XRD), infrared spectroscopic analysis (IR), dc electrical resistivity and Seebeck coefficient which are utilized in order to study the effect of variation of zinc substitution to get the desired concentrations of Mn^{2+} and Zn^{2+} ions to obtain the desired Curie temperature and electric properties to reduce losses to open new era of applications in telecommunications and electronics.

2. Experimental Techniques

Polycrystalline spinel ferrite with formula $Mn_{1-x}Zn_xFe_2O_4$, ($0.0 \le x \le 0.5$ in steps of 0.1) was prepared by a solid state reaction. In this method high purity oxides $MnCO_3$, ZnO and Fe_2O_3 were used in stoichiometric ratio and well ground in agate mortar for 4 h, and pre-sintered in air at 900˚C for 5 h with heating rate 4˚C/min using Lenton UAF 16/5 furnace then slow cooled to room temperature. After that, the samples were grounded again for 3 h and the mixture was pressed into pellets using unaxial press of pressure 1.9×10^8 $N \cdot m^{-2}$, then finally sintered in air at 1300˚C for 15 h with heating rate 2˚C/min. Crystalline phases in different annealed samples were identified using XRD on a Brucker axis D8 diffractometer using the Cu-K_α radiation (λ = 1.5418 Å) radiation and a secondary monochromator in the range 2θ from 10˚ to 80˚. The experimental lattice parameter a_{exp} is calculated by using the relations, $a = d\sqrt{h^2 + k^2 + l^2}$, where d is the interplanner distance and h, k, l are Miller indices of each plane and lattice parameter can be calculated from the slope of linear relation between $1/d$ and $\sqrt{h^2 + k^2 + l^2}$. X-ray density (theoretical density) D_x (g/cm^3) was calculated from the relation, $\left(D_x = 8M/N_A a^3\right)$ where 8 represents the number of molecules in a unit cell of the spinel lattice, M the molecular weight of the sample, a the lattice parameter of the ferrite and N_A is Avogadro's number. The percentage porosity P% was calculated from the relation, $\left(P\% = 1 - D_{app}/D_x\right) \times 100$, where D_{app} is the apparent density. The two surfaces of each pellet were coated with silver paste and checked for good electrical contact. The dc resistivity of the samples was measured using the two probe method. The thermoelectric power (Seebeck coefficient) as a function of temperature was measured across the pellet to determine the type of charge carriers.

3. Results and Discussion

3.1. Structural Properties

3.1.1. X-Ray Diffraction

Sintering process is necessary step in the preparation of ferrite by standard ceramic method, and the sintering temperature plays a key role in crystalline type and particle size of ferrite [13] [14]. **Figure 1** shows the XRD patterns of the prepared ferrite samples indicating that the samples in a single phase cubic spinel structure, which indicates that the crystallographic planes of the characteristic peaks of cubic spinel structure that perfectly matched with the theoretical data of Franklinite spinel structure (ICDD card No. 74-2402). **Figure 2** shows that the positions of peaks were shifted to a higher value of 2θ with substitution of Zn^{2+} ions, indicating that the lattice parameter for the cubic $Mn_{1-x}Zn_xFe_2O_4$ samples decreased with Zn-content (x). The crystallite size (t) of the prepared samples was calculated using Scherrer's Equation [15],

$$t = \left(0.9\lambda/\beta\cos\theta\right) \tag{1}$$

where β is the peak width at half maximum, λ is wavelength and θ corresponds to the peak position. The most intense peak at (220), (311) and (400) are used for calculation. The calculated crystallite size (t) as a function of Zn content (x) shows that the substitution the Mn^{2+} ions by Zn^{2+} ions results in decrease in crystallite size from 115 nm to 90 nm as shown in **Table 1**.

The experimental lattice parameter (a_{exp}) of the prepared samples was calculated and plotted as a function of Zn content (x) which decreases with increasing Zn content (x) in accordance to gradual replacement of bigger Mn^{2+} ions of higher ionic radius (0.75 Å) with smaller Zn^{2+} ions of ionic radius (0.68 Å) as shown in **Figure 3** [16]-[18]. The correlation between the ionic radii and the theoretical lattice constant (a_{th}) is calculated using the equation [19]:

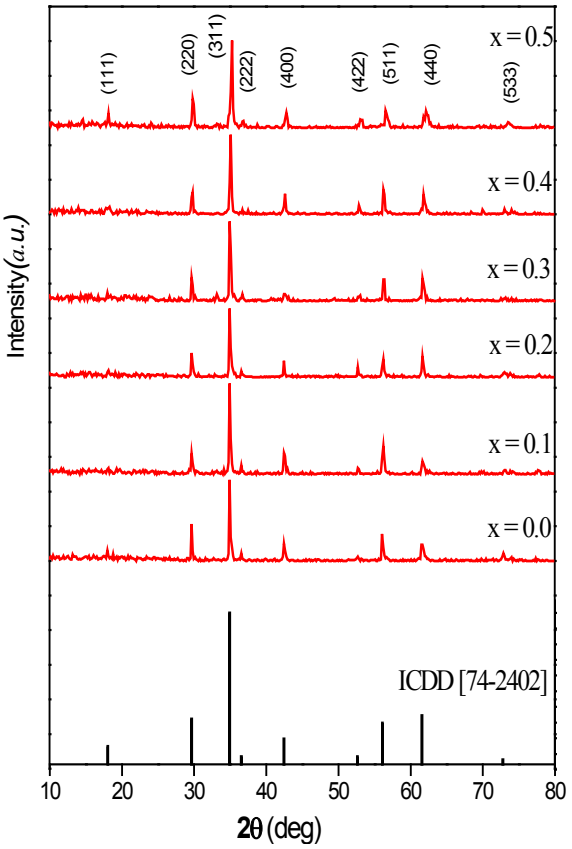

Figure 1. X-ray diffraction patterns and ICDD card for all samples of system $Mn_{1-x}Zn_xFe_2O_4$.

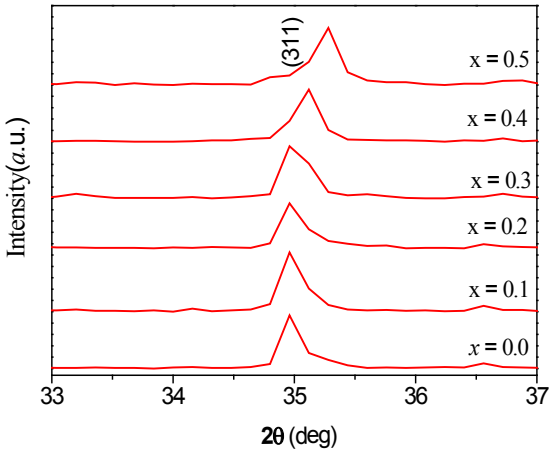

Figure 2. Effect of Zn concentration on expanded (311) patterns of the XRD patterns of $Mn_{1-x}Zn_xFe_2O_4$.

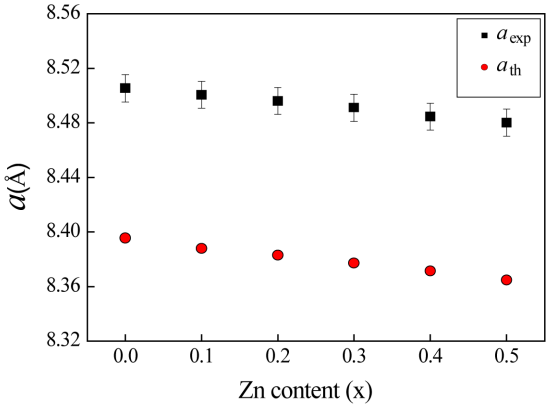

Figure 3. Variation of theoretical (a_{th}) and experimental (a_{exp}) lattice parameter as a function of Zn content (x).

Table 1. Show the effect of Zn-content on the apparent density (D_{app}), X-ray density (D_x) and the crystallite size (t).

Zn-content (x)	Apparent density (D_{app}) g/cm^3	X-ray density (D_x) g/cm^3	Crystallite size (t) nm
0	4.788	4.978	115
0.1	4.781	5.009	108
0.2	4.741	5.04	100.3
0.3	4.743	5.071	96.6
0.4	4.713	5.106	96.5
0.5	4.632	5.135	90.15

$$a_{th} = \frac{8}{3\sqrt{3}}\left[\left(r_A + R_o\right) + \sqrt{3}\left(r_B + R_o\right)\right] \quad (2)$$

where R_o is the radius of the oxygen ion (1.38 Å), r_A and r_B are the ionic radii of tetrahedral A- and octahedral B-site, respectively. In order to calculate r_A and r_B it is necessary to know the cation distribution for a given system. In general, Zn^{2+} ions have higher preference for A-sites while Mn^{2+} and Fe^{3+} ions are distributed between the tetrahedral A- and octahedral B-sites, so the formula of the cation distribution can be written as:

$$(Zn^{2+}{}_x\ Mn^{2+}{}_{0.8-x}\ Fe^{3+}{}_{0.2})[Mn^{2+}{}_{0.2}\ Fe^{3+}{}_{1.8}]O^{2-}{}_4$$

where the brackets ( ) and [ ] denote to A- and B-sites respectively. The ionic radius of each site was calculated according to the following equations:

$$r_A = [(x)\, r_{Zn}^{2+} + (0.8 - x) r_{Mn}^{2+} + (0.2) r_{Fe}^{3+}] \quad (3)$$

$$r_B = 0.5\, [(0.2)\, r_{Mn}^{2+} + (1.8) r_{Fe}^{3+}] \quad (4)$$

where r_{Zn}^{2+}, r_{Mn}^{2+} and r_{Fe}^{3+} are the ionic radii of Zn^{2+}, Mn^{2+} and Fe^{3+} ions respectively. The theoretical and experimental values of lattice parameter (a_{th} and a_{exp}) are plotted against Zn content (x) in **Figure 3**. From **Figure 3**, one can see that (a_{th} and a_{exp}) decreased slightly with increasing Zn content (x). This decrease may be due to substitutional occupancy since the ionic radii of Zn^{2+}, Mn^{2+} and Fe^{3+} ions are 0.68, 0.75 and 0.64 Å respectively. **Figure 3** also shows that the experimental lattice parameter is greater than theoretical lattice parameter; this can be attributed to the formation of Fe^{2+} ions during the sintering process, which have an ionic radius greater than Fe^{3+}.

The X-ray density (D_x) was calculated using the relation [20]:

$$D_x = 8M / Na^3 \quad (5)$$

where 8 is the number of molecules in a unit cell of spinel lattice, M is the molecular weight of the sample, a_{exp} is the experimental lattice parameter of the ferrite and N is the Avogadro's number. The theoretical density D_x depends on the lattice constant and molecular weight of the sample. The theoretical density D_x as a function of Zn concentration is shown in **Figure 4**. It can be seen from the figure that the X-ray density increases with the increase in Zn-content (x), where it is inversely proportional to the lattice constant, which decreases with increasing Zn content. In addition, the difference in atomic weight between Mn (54.938) and Zn (65.37) contributes to this increase in D_x. Pores trapped inside the grains must be explained in terms of rapid grain growth, with increasing the Zn^{2+} ions concentration. It is clear from **Figure 5** that, as Zn content (x) increases the porosity increases this can be explained as follow. It is well known that the porosity of ceramic samples results from two sources namely intragranular (P_{intra}) and intergranular porosity (P_{inter}), so that the total porosity (P%) could be written as the sum of two types

The percentage porosity (P%) was calculated from the relation

$$P\% = \left(1 - D_{app} / D_x\right) \times 100 \quad (6)$$

where D_{app} is the apparent density, it was found that the apparent density D_{app} values are less than those of X-ray density D_x as shown in **Table 1**, such behavior was expected due to the presence of pores formed during sintering process, therefore the replacements of Mn^{2+} ions by Zn^{2+} ions caused a relative decrease in apparent density D_{app} of the sample and a corresponding increase in porosity P%. In addition the decrease of density and the

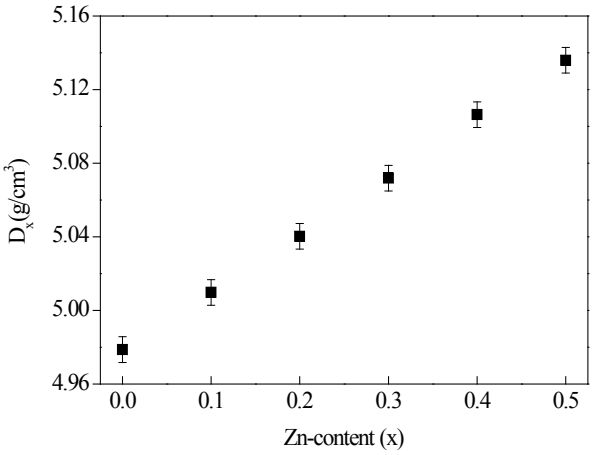

Figure 4. Variation of theoretical density (D_x) as a function of Zn content (x).

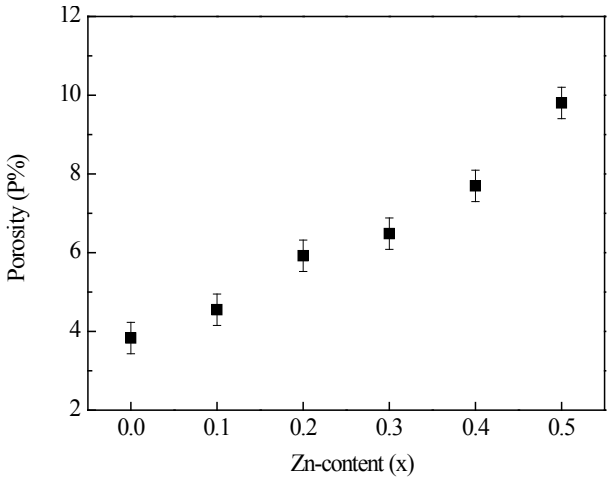

Figure 5. Variation of porosity (*P*%) as a function of Zn content (x).

increase of porosity with increasing Zn content (x) are due to the increase of oxygen vacancies which plays a predominant role in accelerating densification; *i.e.* the decrease in oxygen ion (anion) diffusion would retard the densification. The presence of Zn^{2+} ions reduces the population of Fe^{3+} ions in B-sites resulting in the decrease of density as well as the increase in porosity [21].

3.1.2. Infrared Spectroscopic Analysis (IR)

Figure 6 shows the IR absorption spectra for $Mn_{1-x}Zn_xFe_2O_4$ ($0.0 \le x \le 0.5$), from which it can be seen that there are five bands characterizing spinel ferrites in the range 200 - 1000 cm^{-1} for the observed samples [22]. As seen in **Table 2** the positions of five bands are recorded, the five bands can be classified into two groups; two high-frequency bands and three low-frequency bands. In the high-frequency bands (υ_1) is in range of 547 - 555 cm^{-1} and is related to intrinsic vibrations of tetrahedral group, the second band (υ_2) is in the range of 407 - 430 cm^{-1} and is related to intrinsic vibrations of octahedral group. Band (υ_1) (near 600 cm^{-1}) arises due to tetrahedral complexes (the stretching vibration of tetrahedral metal-oxygen band) and band (υ_2) (near 400 cm^{-1}) is due to octahedral complexes (metal-oxygen vibration in octahedral sites). The difference in position of two strong bands (υ_1) and (υ_2) could be related to difference in Fe^{3+}-O^{2-} distance for A-sites (0.189 nm) and that of the B-sites (0.199 nm). The three low-frequency bands, (υ_3) is in the range 380 - 387 cm^{-1} and is related to the divalent octahedral metal-oxygen ion complexes. The fourth band (υ_4) and fifth band (υ_5) in range 215 - 284 cm^{-1} were observed and can be assigned to the divalent tetrahedral vibrations (lattice vibration). The presence of shoulder (υ') could be ascribed to the linear combination of the bands (υ_2) at 407 cm^{-1} and (υ_3) at 380 cm^{-1} (407 + 380) = 787 cm^{-1} at x = 0.1, (υ_2) at 423 cm^{-1} and (υ_3) at 380 cm^{-1} (423 + 380) = 803 cm^{-1} at x = 0.4 [23]. The data in **Table 2** confirm these results.

3.2. Electrical Properties

3.2.1. D.C. Electrical Resistivity

The electric properties of the ferrite to spinel system $Mn_{1-x}Zn_xFe_2O_4$, was studied for ($0.0 \le x \le 0.5$ in steps of 0.1), over temperature range from room temperature to 650 K and represented in **Figure 7**. **Figure 7** shows the variation of dc resistivity, expressed as (ln ρ) with absolute temperature, expressed as 1000/T. The obtained results could be described according to relation,

$$\rho = \rho_o \exp\left(E/KT\right) \tag{7}$$

where E is the activation energy, K is the Boltzmann constant, ρ_o is the temperature independent constant. The temperature dependence of resistivity exhibits two breaks and distinct regions (I, II and III). Such a break was associated with a change in the slope which is attributed to the change of magnetic order and lowering the generation of charge carrier [24] confirmed this discussion and suggested that the change in the slope can be either

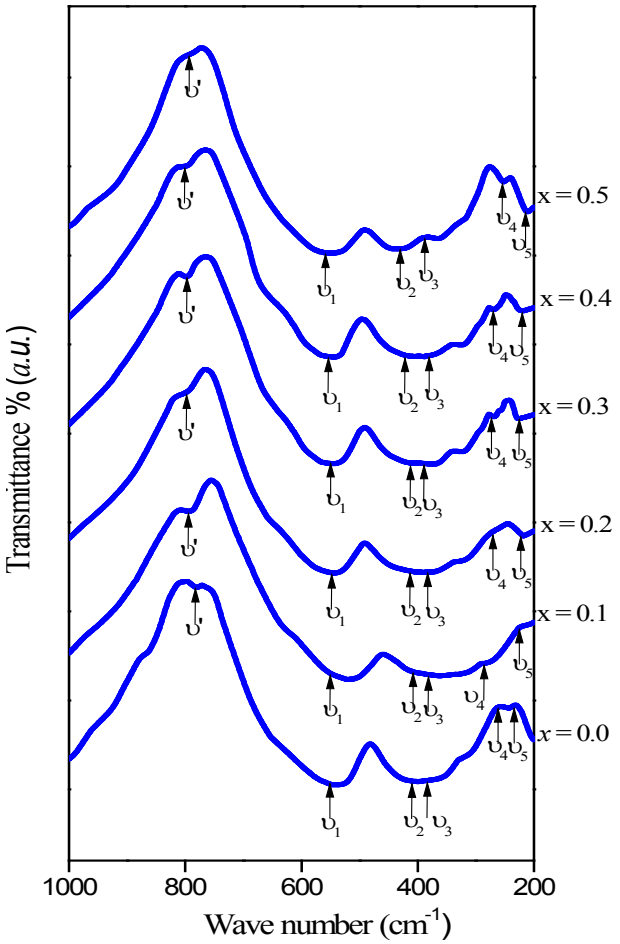

Figure 6. IR transmission spectra for the samples $Mn_{1-x}Zn_xFe_2O_4$ system.

Table 2. Values of transmission bands for ferrites $Mn_{1-x}Zn_xFe_2O_4$ prepared by standard ceramic method where ($0.0 \leq x \leq 0.5$ in steps of 0.1).

Zn-content (x)	υ' cm^{-1}	υ_1 cm^{-1}	υ_2 cm^{-1}	υ_3 cm^{-1}	υ_4 cm^{-1}	υ_5 cm^{-1}
0.0	783	550	409	383	261	223
0.1	793	550	407	380	284	223
0.2	795	547	411	381	268	224
0.3	795	549	410	386	273	226
0.4	799	551	423	380	269	219
0.5	795	555	430	387	255	215

linked with magnetic ordering or with a conduction mechanism. The first region is attributed to extrinsic conduction mechanism (impurities); it extends from room temperature up to the first transition temperature (T_1) ≈ 305:355 K for all studied samples. The second transition temperature $(T_c)_{elec.}$ is always attributed to the magnetic phase transition from ferrimagnetic to paramagnetic state. The activation energies for the conduction process were calculated from slopes of each line according to Equation (8). The activation energies ($E_{ferri.}$) for region II and ($E_{para.}$) for region III and the transition temperature $(T_c)_{elec.}$ between ferrimagnetic and paramagnetic region are given in **Table 3** which are ranged from 396 to 515 K for all samples and agrees with the published data for spinel ferrites. **Figure 8** shows the relation between ($\ln\rho$) and 1000/T for sample (x = 0.2) *i.e.*, $Mn_{0.8}Zn_{0.2}Fe_2O_4$, as an example of studied samples to illustrate the transition temperatures. The change in

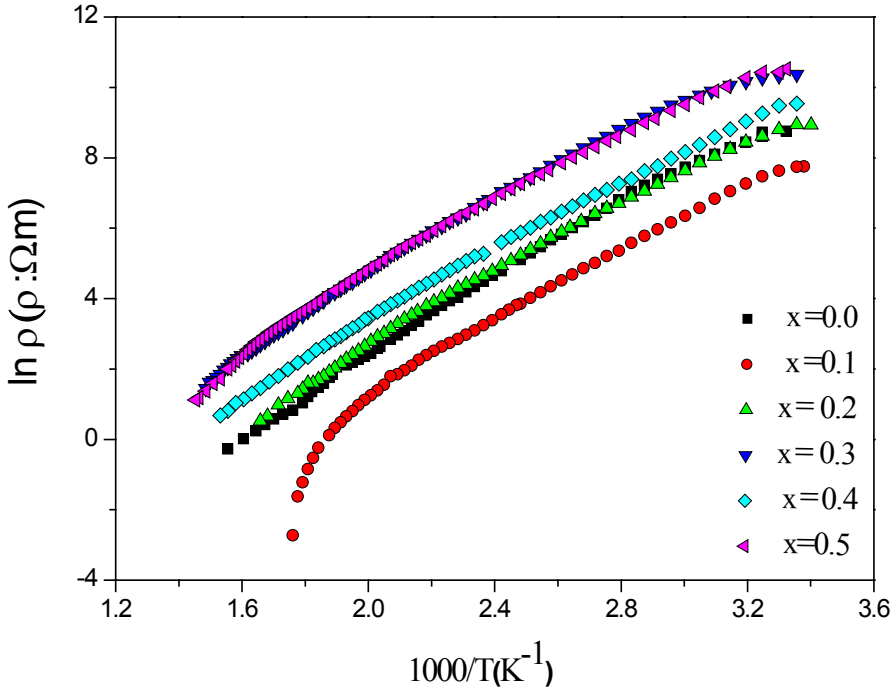

Figure 7. Relation between lnρ and 1000/T of $Mn_{1-x}Zn_xFe_2O_4$ system ($0.0 \le x \le 0.5$).

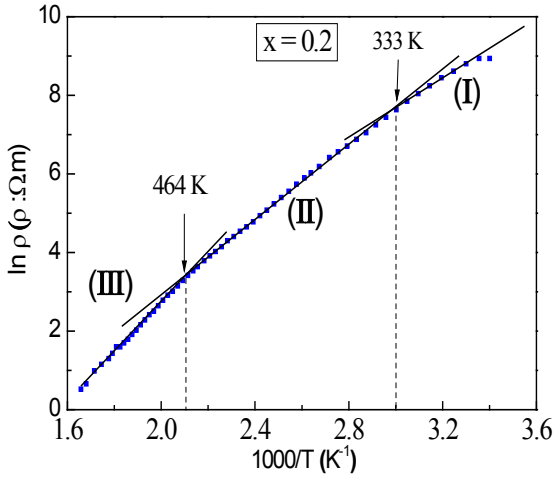

Figure 8. Relation between ln ρ(Ω.m) and 1000/T $(K)^{-1}$ of $Mn_{0.8}Zn_{0.2}Fe_2O_4$ sample.

Table 3. The effect of Zn-content on the activation energies, the transition temperatures and the resistivity at room temperature.

Zn-content (x)	$E_{ferri.}$(eV)II	$E_{para.}$(eV)III	T_1(K)	$T_{c.elect.}$(K)	ρ(Ω.m) × 10^3
0.0	0.45	0.67	355	515	6.3
0.1	0.43	0.81	343	541	2.3
0.2	0.40	0.55	333	464	7.6
0.3	0.39	0.50	333	409	31.9
0.4	0.37	0.50	305	396	13.9
0.5	----	0.41	314	----	36.9

activation energies between region II and region III is attributed to magnetic transition from order to disorder state. It is observed that ($E_{para.}$) is greater than ($E_{ferri.}$) for all investigated samples as shown **Table 3**. The increase of the activation energy from order to disorder state was attributed to the volume expansion above T_c. The lower activation energy in the ferrimagnetic region is attributed to the magnetic spin disordering due to decrease in the concentration of current carriers [25] [26], while the change in activation energy is attributed to the change in conduction mechanism (polaron hopping). This decrease of resistivity in ferrite is due to the exponential increase of drift mobility of charge carriers with temperature.

3.2.2. Seebeck Coefficient

The temperature dependence of Seebeck voltage coefficient for the investigated samples for $Mn_{1-x}Zn_xFe_2O_4$ with $0.0 \le x \le 0.5$ is shown in **Figure 9**. From the figure it is clear that, the investigated samples with negative sign indicates the semiconducting n- type behavior of the samples which is predominantly due to hopping of electron from Fe^{2+} to Fe^{3+} ions ($Fe^{2+} \leftrightarrow Fe^{3+} + e^-$) [27] [28]. It is clear that the number of charge carriers is nearly constant. In other words, increasing Zn^{2+} ion substitution leads to the migration of more Fe^{3+} from tetrahedral site to octahedral one, hence increasing hopping electron between $Fe^{2+} \leftrightarrow Fe^{3+}$. This means that the variation in the conductivity is due to thermally activated mobility and not due to thermal activated creation of charge carriers.

4. Conclusions

1) XRD measurements confirm the formation of single-phase cubic spinel structure;

2) The experimental lattice parameter (a_{exp}) and crystallite size (t) decrease while the porosity (P) increases with increasing Zn^{2+} ions;

3) Dc electrical resistivity and Seebeck voltage coefficients were measured as a function of temperature using the two probe method; it is also found that the temperature variation of resistivity exhibits two breaks, each break referring to a change in the activation energy;

4) The Curie temperature decreases with increasing Zn^{2+} ions;

5) Seebeck voltage coefficients measurements reveal n-type conduction for all samples.

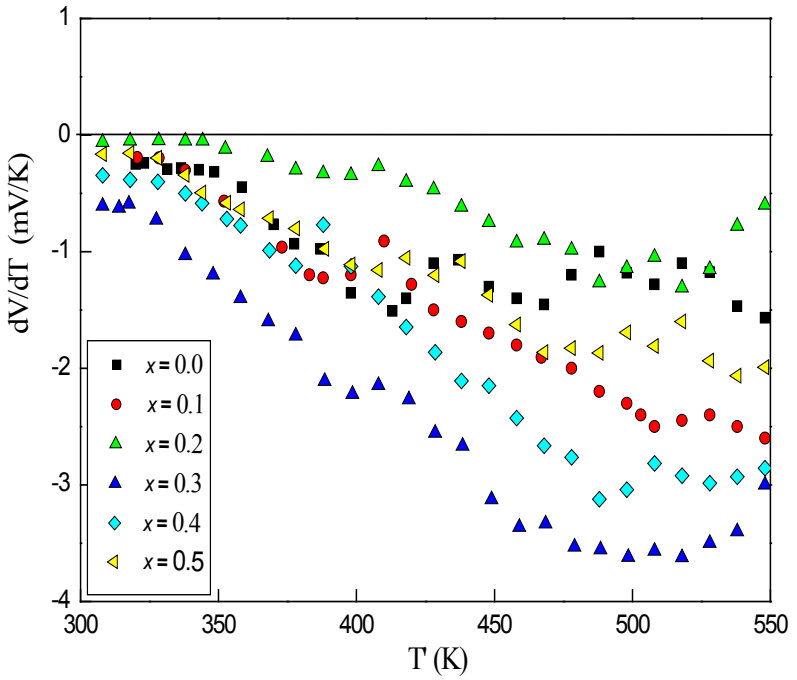

Figure 9. Seebeck voltage coefficient as a function of the average temperature of $Mn_{1-x}Zn_xFe_2O_4$ system ($0.0 \le x \le 0.5$).

5. Highlights

The investigated samples $Mn_{1-x}Zn_xFe_2O_4$ ($0.0 \leq x \leq 0.5$ in steps of 0.1) showed that:

- Dc electrical resistivity increased from (2.3 - 36.9) × 10^3 Ω.m with increasing Zn^{2+} ions;
- The Curie temperature decreases with increasing Zn^{2+} ions;
- Seebeck voltage coefficients measurements reveal n-type conduction for all samples.

So we recommend sample x = 0.5 in many applications due to higher resistivity.

References

[1] Arulmurugan, R., Jeyadevan, B., Vaidyanathan, G. and Sendhilnathan, S. (2005) Effect of Zinc Substitution on Co-Zn and Mn-Zn Ferrite Nanoparticles Prepared by Co-Precipitation. *Journal of Magnetism and Magnetic Materials*, **288**, 470-477. http://dx.doi.org/10.1016/j.jmmm.2004.09.138

[2] Fujioka, H., Ikeda, T., Ono, K., Ito, S. and Oshima, M. (2002) Characteristics of InSb Grown on Single Crystalline Mn-Zn Ferrite Substrates. *Journal of Crystal Growth*, **241**, 309-312. http://dx.doi.org/10.1016/S0022-0248(02)01311-8

[3] Sathishkumar, G., Venkataraju, C. and Sivakumar, K. (2010) Synthesis, Structural and Dielectric Studies of Nickel Substituted Cobalt-Zinc Ferrite. *Materials Sciences and Applications*, **1**, 19-24. http://dx.doi.org/10.4236/msa.2010.11004

[4] Taylor, J.A.T., Reczek, S.T. and Rosen, A. (1995) Soft Ferrite Processing. *American Ceramic Society Bulletin*, **74**, 91.

[5] Wang, J., Zeng, C. Peng, Z. and Chen, Q. (2004) Synthesis and Magnetic Properties of $Zn_{1-x}Mn_xFe_2O_4$ Nanoparticles. *Physica B*: *Condensed Matter*, **349**, 124-128. http://dx.doi.org/10.1016/j.physb.2004.02.014

[6] Ott, G., Wrba, J. and Lucke, R. (2003) Recent Developments of Mn-Zn Ferrites for High Permeability Applications. *Journal of Magnetism and Magnetic Materials*, **254-255**, 535-537. http://dx.doi.org/10.1016/S0304-8853(02)00961-7

[7] Yu, Z., Sun, K., Li, L., Liu, Y., Lan, Z. and Zhang, H. (2008) Influences of Bi_2O_3 on Microstructure and Magnetic Properties of MnZn Ferrite. *Journal of Magnetism and Magnetic Materials*, **320**, 919-923. http://dx.doi.org/10.1016/j.jmmm.2007.09.008

[8] Ghazanfar, U., Siddiqi, S.A. and Abbas, G. (2005) Structural Analysis of the Mn-Zn Ferrite, Using XRD Technique. *Materials Science and Engineering B*, **118**, 84-86. http://dx.doi.org/10.1016/j.mseb.2004.12.018

[9] Hessien, M.M., Rashad, M.M., El-Barawy, K. and Ibrahim, I.A. (2008) Influence of Manganese Substitution and Annealing Temperature on the Formation, Microstructure and Magnetic Properties of Mn-Zn Ferrites. *Journal of Magnetism and Magnetic Materials*, **320**, 1615-1621. http://dx.doi.org/10.1016/j.jmmm.2008.01.025

[10] Kim, S.J., Hyun, S.W., Kim, C.S. and Kim, H.J. (2014) Thermal Variation of MgZn Nanoferrites for Magnetic Hyperthermia. *Journal of the Korean Physical Society*, **65**, 553-556. http://dx.doi.org/10.3938/jkps.65.553

[11] Akther Hossaina, A.K.M., Mahmuda, S.T., Sekib, M., Kawaib, T. and Tabata, H. (2007) Structural, Electrical Transport, and Magnetic Properties of $Ni_{1-x}Zn_xFe_2O_4$. *Journal of Magnetism and Magnetic Materials*, **312**, 210-219. http://dx.doi.org/10.1016/j.jmmm.2006.09.030

[12] Zaki, H.M. (2009) The Influence of Zn Ions Substitution on the Transport Properties of Mg-Ferrite. *Physica B*: *Condensed Matter*, **404**, 3356-3362. http://dx.doi.org/10.1016/j.physb.2009.05.012

[13] Lv, W.Z., Liu, B., Luo, Z.K., Ren, X.Z. and Zhang, P.X. (2008) XRD Studies on the Nanosized Copper Ferrite Powders Synthesized by Sonochemical Method. *Journal of Alloys and Compounds*, **465**, 261-264. http://dx.doi.org/10.1016/j.jallcom.2007.10.049

[14] Zhang, C.F., Zhong, X.C., Yu, H.Y., Liu, Z.W. and Zeng, D.C. (2009) Effects of Cobalt Doping on the Microstructure and Magnetic Properties of Mn-Zn Ferrites Prepared by the Co-Precipitation Method. *Physica B*: *Condensed Matter*, **404**, 2327-2331. http://dx.doi.org/10.1016/j.physb.2008.12.044

[15] Kigery, W.D., Bowen, H.K. and Uhlmann, D.R. (1975) Introduction of Ceramics. John Wiley & Sons, New York, 458.

[16] Nalbandian, L., Delimitis, A., Zaspalis, V.T., Deliyanni, E.A., Bakoyannakis, D.N. and Peleka, E.N. (2008) Hydrothermally Prepared Nanocrystalline Mn-Zn Ferrites: Synthesis and Characterization. *Microporous and Mesoporous Materials*, **114**, 465-473. http://dx.doi.org/10.1016/j.micromeso.2008.01.034

[17] Rath, C., Anand, S., Das, R.P., Sahu, K.K., Kulkarni, S.D., Date, S.K. and Mishra, N.C. (2002) Dependence on Cation Distribution of Particle Size, Lattice Parameter, and Magnetic Properties in Nanosize Mn-Zn Ferrite. *Journal of Applied Physics*, **91**, 2211-2215. http://dx.doi.org/10.1063/1.1432474

[18] Shannon, R.D. (1976) Revised Effective Ionic Radii and Systematic Studies of Interatomic Distances in Halides and Chalcogenides. *Acta Crystallographica Section A*, **32**, 751-767. http://dx.doi.org/10.1107/S0567739476001551

[19] Heiba, Z.K., Mohamed, M.B., Ahmed, M.A., Moussa, M.A.A. and Hamdeh, H.H. (2014) Cation Distribution and Dielectric Properties of Nanocrystalline Gallium Substituted Nickel Ferrite. *Journal of Alloys and Compounds*, **586**, 773-

781. http://dx.doi.org/10.1016/j.jallcom.2013.10.137

[20] Eltabey, M.M., Ali, I.A., Hassan, H.E. and Comsan, M.N.H. (2011) Effect of γ-Rays Irradiation on the Structure and Magnetic Properties of Mg-Cu-Zn Ferrites. *Journal of Materials Science*, **46**, 2294-2299. http://dx.doi.org/10.1007/s10853-010-5071-6

[21] Ahmed, M.A. and Okasha, N. (2009) Role of Cu^{2+} Concentration on the Structure and Transport Properties of Cr-Zn Ferrites. *Journal of Magnetism and Magnetic Materials*, **321**, 3436-3441. http://dx.doi.org/10.1016/j.jmmm.2009.06.041

[22] Hemeda, O.M. (2004) IR Spectral Studies of $Co_{0.6}Zn_{0.4}Mn_xFe_{2-x}O_4$ Ferrites. *Journal of Magnetism and Magnetic Materials*, **281**, 36-41. http://dx.doi.org/10.1016/j.jmmm.2004.01.100

[23] Ahmed, M.A., Ateia, E. and El-Dek, S.I. (2002) Spectroscopic Analysis of Ferrite Doped with Different Rare Earth Elements. *Vibrational Spectroscopy*, **30**, 69-75. http://dx.doi.org/10.1016/S0924-2031(02)00040-1

[24] Satter, A.A., El-Sayed, H.M. and El-Tabey, M.M. (2005) The Effect of Al-Substitution on Structure and Electrical Properties of Mn-Ni-Zn Ferrites. *Journal of Materials Science*, **40**, 4873-487. http://dx.doi.org/10.1007/s10853-005-3884-5

[25] Murugesan, M., Ishigaki, T., Kuwano, H., Chen, M., Liu, R.S. and Nachimuthu, P. (1999) Enhancement of Critical Pr Ion Concentration(xcr) in $(La_{1-x}Pr_x)Ba_2Cu_3O_z$. *Journal of Applied Physics*, **86**, 6985-6992. http://dx.doi.org/10.1063/1.371783

[26] Abo-Arais, A. and Dawoud, M.A.T. (2005) New Phases of YBaCuGeO Superconductors Identified from X-Ray Diffraction and Infra-Red Absorption Measurements. *Turkish Journal of Physics*, **29**, 33-41.

[27] Solyman, S. (2006) Transport Properties of La-Doped Mn-Zn Ferrite. *Ceramics International*, **32**, 755-760. http://dx.doi.org/10.1016/j.ceramint.2005.05.018

[28] Ahmed, M.A., Ateia, E., Salah, L.M. and El-Gamal, A.A. (2005) Structural and Electrical Studies on La^{3+} Substituted Ni-Zn Ferrites. *Materials Chemistry and Physics*, **92**, 310-321. http://dx.doi.org/10.1016/j.matchemphys.2004.05.049

Scientific Research Publishing (SCIRP) is one of the largest Open Access journal publishers. It is currently publishing more than 200 open access, online, peer-reviewed journals covering a wide range of academic disciplines. SCIRP serves the worldwide academic communities and contributes to the progress and application of science with its publication.

Other selected journals from SCIRP are listed as below. Submit your manuscript to us via either submit@scirp.org or Online Submission Portal.